JACS
JOURNAL OF THE AMERICAN CHEMICAL SOCIETY

Article

pubs.acs.org/JACS

Sequence-Specific Electrical Purification of Nucleic Acids with Nanoporous Gold Electrodes

Pallavi Daggumati,[†] Sandra Appelt,[‡] Zimple Matharu,[†] Maria L. Marco,[‡] and Erkin Seker*[,†]

[†]Department of Electrical and Computer Engineering and [‡]Department of Food Science & Technology, University of California, Davis, California 95616, United States

Supporting Information

ABSTRACT: Nucleic-acid-based biosensors have enabled rapid and sensitive detection of pathogenic targets; however, these devices often require purified nucleic acids for analysis since the constituents of complex biological fluids adversely affect sensor performance. This purification step is typically performed outside the device, thereby increasing sample-to-answer time and introducing contaminants. We report a novel approach using a multifunctional matrix, nanoporous gold (np-Au), which enables both detection of specific target sequences in a complex biological sample and their subsequent purification. The np-Au electrodes modified with 26-mer DNA probes (via thiol−gold chemistry) enabled sensitive detection and capture of complementary DNA targets in the presence of complex media (fetal bovine serum) and other interfering DNA fragments in the range of 50−1500 base pairs. Upon capture, the non-complementary DNA fragments and serum constituents of varying sizes were washed away. Finally, the surface-bound DNA−DNA hybrids were released by electrochemically cleaving the thiol−gold linkage, and the hybrids were iontophoretically eluted from the nanoporous matrix. The optical and electrophoretic characterization of the analytes before and after the detection−purification process revealed that low target DNA concentrations (80 pg/μL) can be successfully detected in complex biological fluids and subsequently released to yield pure hybrids free of polydisperse digested DNA fragments and serum biomolecules. Taken together, this multifunctional platform is expected to enable seamless integration of detection and purification of nucleic acid biomarkers of pathogens and diseases in miniaturized diagnostic devices.

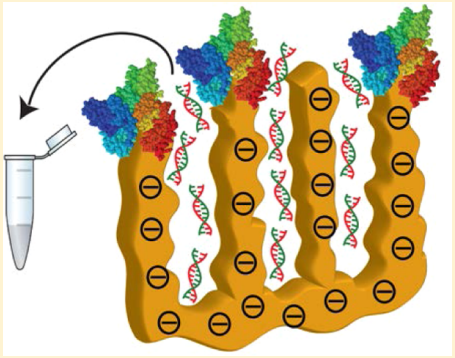

INTRODUCTION

With the advent of nanostructured materials, nucleic-acid-based biosensors for pathogen detection have exhibited enormous progress during the past decade.[1−3] Miniaturization of the sensor platform coupled with phenomena unique to nanoscale[4] enabled faster sensor response, lower limits of detection, and reduced reagent volumes compared to traditional benchtop methods.[5,6] However, in order to benefit from these features, most sensing platforms still require sample preparation, particularly purification of nucleic acids from complex biological samples.[7] Traditional benchtop (off-chip) processes for DNA extraction often utilize phase separation, where proteins in the complex sample are denatured or aggregated, DNA is precipitated with alcohols or physisorbed to a solid-phase support, and DNA is finally recovered through centrifugation or elution.[8,9] To achieve a complete sample-in−answer-out system, it is imperative to integrate sample preparation and detection modalities. While DNA capture via solid-phase supports, such as ones created by packing microfluidic channels with silica beads or embedding the beads in sol−gel matrices,[10,11] is more conducive to integration into miniaturized nucleic acid interrogation platforms, these devices still suffer from mechanical instability, including matrix shrinkage compromising DNA extraction efficiency.[12,13] To mitigate the mechanical issues and low reproducibility while maintaining a high surface-area-to-volume ratio for efficient DNA capture, top-down photolithographic approaches were used to incorporate pillars in microfluidic channels[14] with various materials, including silica,[15] poly(methyl methacrylate),[16] and polycarbonate.[17] However, the complex microfabrication processes to create these high-aspect-ratio structures have limited their feasibility. Other nontraditional techniques such as use of paramagnetic particles[18] and hydrophobic magnetic ionic liquids[19] for magnetic capture and release of DNA presented procedural challenges that required complex system design to incorporate magnets required for DNA capture. In summary, a major obstacle to realizing sample-in−answer-out platforms remains to be the lack of seamless integration of sample preparation and analysis modalities.

To address this significant need, we present a novel approach for integrated electrical detection and purification of DNA in complex biological samples using nanoporous gold (np-Au) as a multifunctional electrode coating. Owing to its catalytic properties, tunable morphology, microfabrication compatibility, and excellent thiol−gold chemistry, np-Au is an emerging material for biosensing applications.[20−22] We recently demonstrated that np-Au electrochemical sensors exhibit excellent

Received: April 6, 2016
Published: May 31, 2016

ACS Publications © 2016 American Chemical Society

DOI: 10.1021/jacs.6b03563
J. Am. Chem. Soc. 2016, 138, 7711−7717

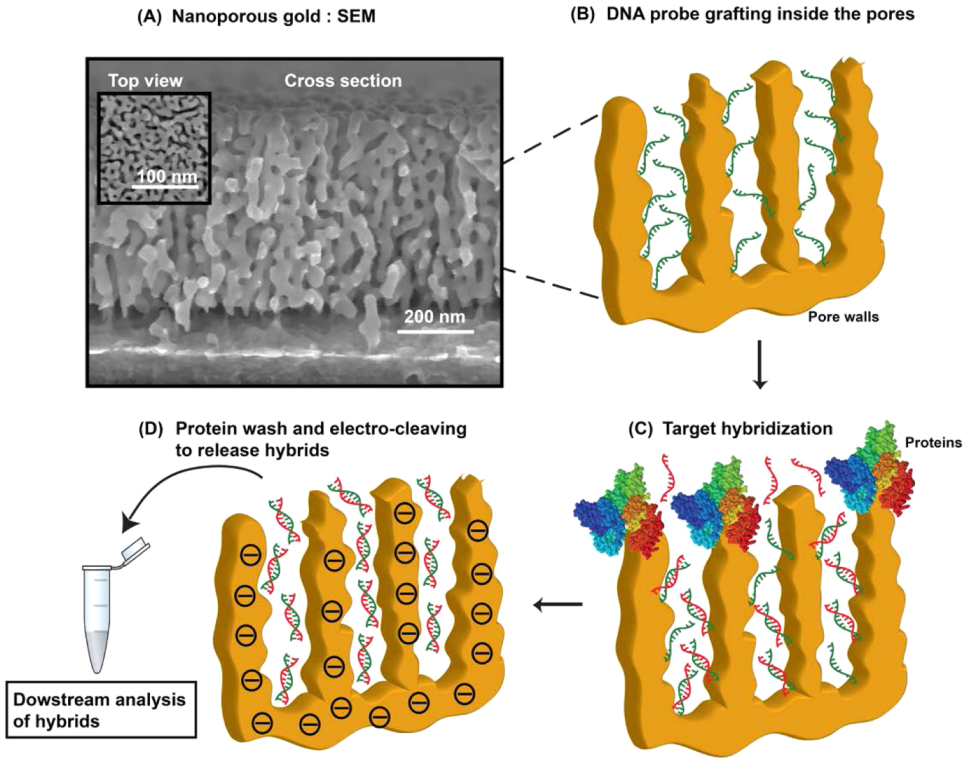

Figure 1. (A) Scanning electron micrographs of np-Au electrode. (B) Thiol-immobilized ssDNA capture probes inside the porous structure. (C) Selective transport of target molecules into the pores while macromolecules (e.g., proteins and other components of FBS) are blocked at the pore entrances. (D) Protein wash and electrochemical cleaving of DNA−DNA hybrids in a low ionic strength buffer. Downstream analysis of eluted hybrids via fluorescence (hybrid concentration), absorbance (DNA-to-protein concentration ratio), and capillary electrophoresis (hybrid size and purity).

biofouling resilience in the presence of complex media such as serum while preserving the sensitive DNA detection capabilities.[23,24] In addition, because the np-Au thin film electrodes can be easily produced using conventional microfabrication techniques, they are highly amenable to seamless integration with microfluidics and other microsystem components to build complete sample-in−answer-out platforms.[25] Leveraging these features, the two-part purification approach demonstrated here enables both the electrochemical detection of DNA targets of interest in the presence of complex media (fetal bovine serum, FBS) as well as subsequent electrokinetic release of the DNA−DNA hybrids free of contaminants (e.g., serum macromolecules and mismatched DNA fragments) for additional downstream analysis.

RESULTS AND DISCUSSION

Concept of the Purification Device. The np-Au electrodes were fabricated using a hybrid approach that merges conventional microfabrication processes and self-assembled nanostructured material synthesis, as described previously.[24] Morphological characterization via scanning electron microscopy (SEM) and subsequent image analysis revealed a median pore radius of 15 nm. (Figure 1A). The residual silver in np-Au samples after dealloying was estimated to be ∼8% (at. %) via energy dispersive spectroscopy (EDS). The concept of capture and electrochemical detection of target DNA molecules, followed by electrokinetic release of the hybrids, is illustrated in Figure 1. To characterize the platform, we used a unique 26-mer housekeeping region of the DNA sequence of tobacco mosaic virus (TMV) as a target sequence. The np-Au electrodes were functionalized with thiolated ssDNA (26-mer) specific to the target of interest (i.e.,TMV). The details of the DNA sequence, sensor preparation, and electrochemical setup are described in the Experimental Methods section. Methylene blue (MB) redox marker was used for quantifying the extent of target hybridization. The electrode was challenged with a complex mixture (FBS solution (10%) spiked with specific 26-mer target DNA and/or DNA digests containing several DNA fragments with strand length of 50−1500 bp). Previous studies by us and others have suggested that macromolecules in FBS, such as globular proteins (e.g., albumin), are too large to go through the np-Au pores whereas the short, fiber-like, nucleic acids can penetrate the porous network, thereby rendering np-Au electrodes biofouling-resilient.[23,26] Owing to this selective transport, it is possible to electrochemically characterize probe−target hybridization of specific target sequences. The large biomolecules (present in FBS) and nonhybridized DNA fragments were then washed away using phosphate buffer. The captured nucleic acids were released by electrochemically cleaving the thiol−gold bond.[27] Desorption of the hybrids was confirmed by an optical assay utilizing PicoGreen, which is a probe that forms a highly fluorescent complex upon specific binding with double-stranded DNA (dsDNA).[28] We further evaluated the efficacy of the purification process by performing capillary electrophoresis on the samples before and after purification.

Target Capture and Electrokinetic Release of Hybrids. In this section, we discuss the results of the electrical purification process and various parameters optimized to improve the DNA extraction. We used MB redox marker for electrochemical DNA detection and quantification because of

DOI: 10.1021/jacs.6b03563
J. Am. Chem. Soc. 2016, 138, 7711−7717

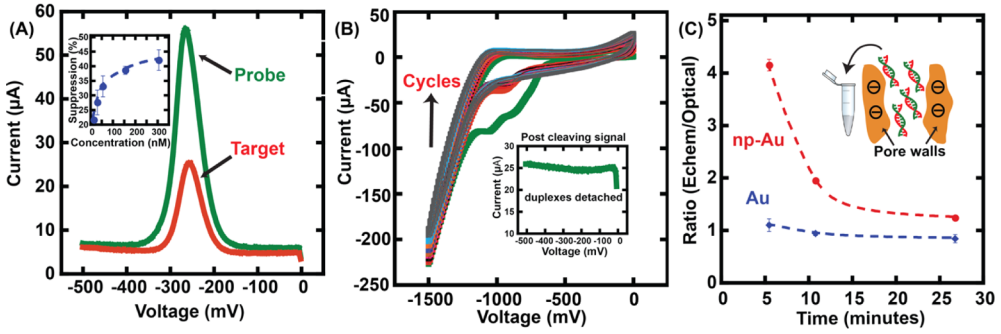

Figure 2. (A) Target DNA detection: Square wave voltammograms (SWV) of probe DNA and target DNA after hybridization. The difference in peak current (at ca. −265 mV) is used to quantify the extent of hybridization. Inset: Target hybridization calibration curve where signal suppression is $(I_{probe} - I_{target}/I_{probe}) \times 100$. (B) Hybrid cleaving: CV in 25 mM phosphate buffer (hybrid elution buffer) at 10 mV/s. Inset: SWV signal after hybrid cleaving. Absence of a reduction peak indicates that DNA hybrids are not anchored onto the surface. (C) Ratio (electrochemical hybrid density estimate to optical hybrid density estimate) vs the duration at reductive negative potentials for each scan rate. Inset: ratio (electrochemical hybrid density estimate to optical hybrid density estimate) vs CV scan rate on np-Au and planar Au electrodes.

its reaction-limited nature (hence its ability to permeate the porous structure before being fully depleted at the top surface) and its ability to discriminate dsDNA from single-stranded DNA (ssDNA).[29] The np-Au electrodes were immobilized with ssDNA probes, and their response to MB was interrogated via square wave voltammetry (SWV) to reduce the influence of significant capacitive current due to the large effective surface area of the np-Au electrodes. All stated electrochemical potentials are with reference to Ag/AgCl electrode. The total number of grafted probes was estimated to be 4.3×10^{12} molecules, which translates into a grafting density that is 10 times that of its planar gold counterpart.[24] This 10-fold increase in the grafting density is in agreement with the surface area enhancement, indicating that most of the porous surface of the electrode is covered with recognition molecules and that MB molecules can access the deeper surfaces of the porous electrode.[24] We then challenged the sensor with the DNA target spiked into FBS solution to simulate the complex environment. We used a loading concentration of 300 nM (2.4 ng/μL) because this corresponds to the concentration that led to sensor saturation in our previous study.[24] Upon target hybridization, the SWV peak current dropped, indicating successful target hybridization (Figure 2A). The number of resultant hybrids was estimated by multiplying the percent signal suppression by the total number of ssDNA with the assumption that the majority of the signal drop is due to the hybridized probes.[29] This was followed by washing off the FBS constituents and electrochemical cleaving to release the thiol-bound hybrids via cyclic voltammetry (CV).

Onset of the thiol bond reduction typically occurs around −0.65 V,[27] but it has been shown that desorption of surface-bound thiolated molecules happens with much higher efficiency at −1.3 V.[30] To that end, in order to ensure complete removal of the surface-bound hybrids and to minimize their readsorption, we used CV in the range of 0 to −1.5 V at scan rates between 10 and 50 mV/s (Figure 2B). Even though the release of hybrids from planar surfaces (e.g., planar gold[27] and indium tin oxide)[31] is almost instantaneous, for the case of np-Au, transport of the desorbed hybrids through the porous structure is hindered as a result of surface−molecule interactions and tortuosity of the np-Au electrode.[32] We therefore employed multiple CV cycles at negative potentials to enhance iontophoretic elution of the negatively charged hybrids into a 25 mM phosphate buffer.[33] There was no SWV peak present after the cleaving process (Figure 2B inset), indicating the successful desorption of the duplexes from the np-Au surfaces. To confirm that the loss of electrochemical signal was due to the absence of duplexes rather than the residual redox molecules, the sensor was further interrogated via SWV following additional MB loading. Observation of a broad peak (Figure S1) confirmed that this signal is mostly due to surface−MB reactions.

Quantification of Duplex Elution Efficiency. Desorption and elution of hybrids was further confirmed by adding PicoGreen stain (Thermo Fisher Scientific) to the eluted hybrids. The concentration of the eluted hybrids was then determined via fluorospectrometry (Nanodrop 3300) (dye calibration details are in Figure S2). The ratio of the electrochemically determined hybrid concentration (extracted from the SWV signal suppression) to the optically determined hybrid concentration with respect to varying cyclic voltammetry scan rates was estimated. The ratio serves as an indicator of duplex elution efficiency. A ratio closer to 1 indicates that the electrochemical hybrid density estimate matches well with the optical estimate, suggesting that majority of the duplexes are desorbed and released into the elution buffer. In case of planar gold, this ratio is independent of the scan rate because the duplexes are not hindered by the presence of a porous network, that is, once the thiol link is cleaved, the duplexes are released straight into the elution buffer. However, in the case of np-Au, the ratio increases as scan rate increases; at high scan rates, desorption is not efficient because the duplexes do not have enough time to exit the entire porous structure. At 10 mV/s, the duration spent (26 min) at negative potentials above the critical thiol reduction potential is long enough for the cleaved duplexes to exit the porous structure (Figure 2C). Consequently, for this scan rate the ratio approaches ∼1, indicating mostly complete elution of the desorbed hybrids. In contrast, when the duplexes were detached by using dithiothreitol (DTT), a common thiol-bond cleaving agent, and no negative potential was applied, the elution of the detached duplexes was significantly hindered (Figure S3). Further investigation of the effect of the number of cycles and cleaving steps, as illustrated in the Supporting Information, revealed that for CV at 10 mV/s and 20 cycles, the optimized ratio was 1.23. These conditions were used for subsequent studies.

Target Capture Efficiency. Another performance metric for the sensing−purification platform is target capture

DOI: 10.1021/jacs.6b03563
J. Am. Chem. Soc. 2016, 138, 7711−7717

efficiency, which is the amount of eluted hybrids recovered after purification as a percentage of the initial target loading concentration (i.e., target DNA of interest spiked into FBS). This is an important metric because the ability to capture and purify low levels of a DNA target is essential for detection and further characterization of biomarkers. For the initial sensing step, np-Au sensor exhibited a dynamic range of detection between 10 and 150 nM and signal saturation at 150 nM with a signal suppression of ∼40% (Figure 3). For the purification

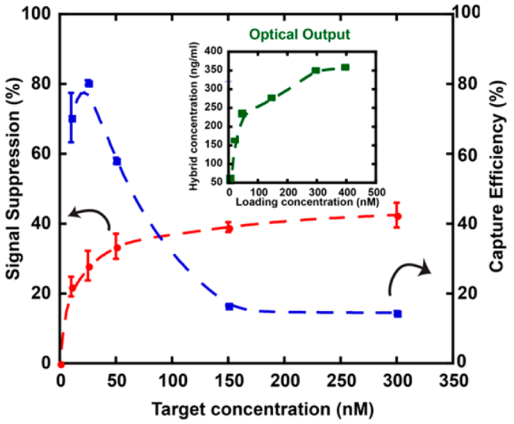

Figure 3. Electrochemical signal suppression as a function of target loading concentration; target capture efficiency = (Hybrid concentration in eluate/target loading concentration) × 100. Inset: hybrid concentration in eluate determined by fluorescence characterization of the duplexes with respect to the target loading concentration.

step, the optical quantification of the eluted duplexes revealed that the target capture efficiency decreased from ∼75% at lower target loading concentrations to ∼15% at high concentrations (Figure 3). The substantial decrease in the capture efficiency for high loading concentrations is attributed to the saturation of the capture probes on the np-Au network. In other words, there remains an appreciable amount of unhybridized target DNA that is removed during the wash step, whereas at low concentrations, a significant portion of the loaded target DNA hybridizes with the probes and is subsequently released from the np-Au electrode. To assess the efficiency in removing proteins during the purification step, we acquired the absorbance values at 260 nm (characteristic to DNA) and 280 nm (characteristic to proteins). The resulting absorbance ratio, A_{260}/A_{280} (with 1.8 generally indicating high purity), is indicative of the relative amount of protein contaminants in DNA samples.[34] The A_{260}/A_{280} ratio was 0.86 ± 0.09 before purification, indicating a strong presence of proteins in the loading solution. Following the purification step, the ratio improved to 1.85 ± 0.06, highlighting that the eluate predominantly contained DNA hybrids free of proteins.

Performance in the Presence of Interfering DNA. A major challenge in detecting specific target sequences in a cell lysate is the presence of DNA fragments of different lengths, sequences, and concentrations. To mimic this scenario, we created a sample mixture model that consists of digested DNA fragments from *Lactobacillus plantarum* (a commensal bacterium common to plants, foods, and intestinal environments), FBS (10%), and the aforementioned specific TMV-derived DNA target. The genomic DNA from *L. plantarum* was partially digested by a DNase for 30 s, at which time digestion was stopped by heat inactivation of the enzyme. We challenged the np-Au sensing-purification platform with this complex sample to assess its detection and purification performance. As for detection, a signal suppression of ∼40% was observed upon hybridization, indicating resilience to the presence of additional fragments and cellular fragments. To assess whether the purification process removed nonspecific DNA fragments of various sizes in the eluate, we performed capillary electrophoresis on the sample model (before subjecting it to purification) and on the eluted hybrids (assay details in the Experimental Methods section). The total DNA amount for each case was kept the same by adjusting the concentration of the supplemented DNA fragments to 2.4 ng/μL, which is at the higher end of the concentrations that the sensor can detect. The electropherograms (represented in traditional gel format) reveal multiple bands corresponding to various input DNA fragments before the sample purification (lanes A and C in Figure 4). In addition, lane C indicates significant signal (darker

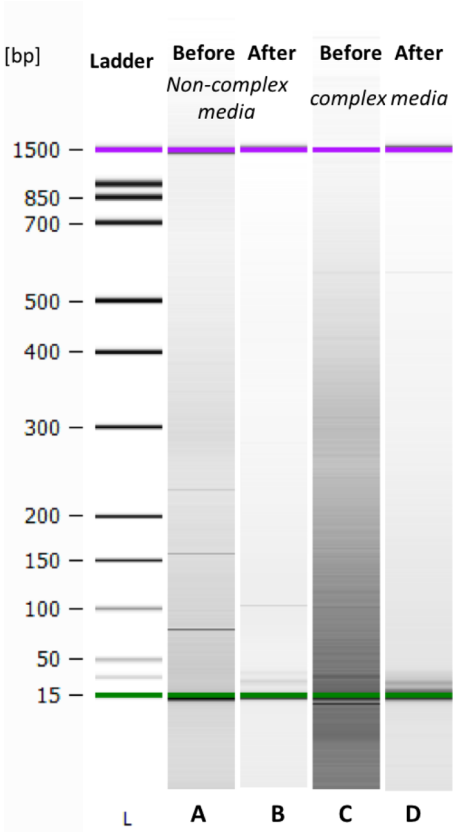

Figure 4. (A) Digested DNA fragments obtained from *L. plantarum* were added to FBS/phosphate buffer and spiked with the 26-mer DNA target. Lane L shows the ladder with different sizes of DNA used for calibration. The upper and lower markers of the ladder are located at 15 and 1500 bp indicated by the green and violet bands on the gel, respectively. Noncomplex media: Gel lanes A and B correspond to the case where np-Au detection and purification device was used in the absence of FBS. The sample before purification containing the added genomic DNA fragments and the desired 26-mer target DNA can be seen in the lane A. After purification, nonspecific DNA fragments in the eluent are removed, and the band corresponding to specific 26-mer DNA hybrids becomes dominant in lane B. Lanes C and D correspond to bands before and after purification in the presence of FBS. Lane D demonstrates that the nonspecific fragment DNA and FBS components are largely eliminated and only the size around the 26-mer target DNA remains.

DOI: 10.1021/jacs.6b03563
J. Am. Chem. Soc. 2016, 138, 7711−7717

bands), possibly from FBS constituents. The subsequent purification step effectively eliminates these bands, and distinctive bands around the size of the 26-mer target DNA appear in lanes B and D (Figure 4). The fluorescent dye binds strongly to dsDNA; therefore, single-stranded target 26-mer DNA is not visualized before purification. On the contrary, after purification, distinct bands corresponding to 26-mer hybrids appear. This is a strong indication that these are in fact 26-mer dsDNA and that the np-Au device was successful in capturing the specific sequence of interest in the presence of competing nonspecific genomic DNA of varying sizes. It should be noted that at high ionic strengths DNA hybridization efficiency is higher as a result of the cation-based electrical screening of the negatively charged DNA backbone thereby reducing repulsion between probe and target strands. This may lead to decreased selectivity in target capture of the exact complementary sequence. It is plausible that the selectivity can be enhanced by identifying ionic strengths that minimize the hybridization of targets with slight mismatches. In addition, the drastic difference between the number and intensity of bands in columns A and B in contrast to those in C and D suggests that the purification step is successful in not only removing FBS components and other DNA fragments but also releasing the duplexes of the specific target DNA. For a semiquantitative comparison of the size distribution for pre- and postpurification samples, we extracted full width at half-maximum (FWHM) and full width at fourth-maximum (FWFM) via intensity analysis of the gels (Figure S4). The FWHM and FWFM centered around the target peak (26 bps) reduced from 150 and 400 bp, respectively, compared to to 13 and 26 bp, respectively, after purification, highlighting successful extraction of the target duplex size.

■ CONCLUSIONS

We demonstrated a novel platform that leverages the unique features of np-Au electrodes (i.e., biofouling resilience and lower limit of detection) to achieve integrated detection and purification of target DNA for further downstream bioanalytical analyses, such as generating specific primers for polymerase chain reaction based sensing schemes and for isolating small DNA/RNA sequences from mixed nucleic acid populations. The electrochemical desorption technique should allow for selective elution of different probe−target pairs or the backfill molecules by modifying the linker chemistry (e.g., using selenol groups instead of thiol groups for certain types of molecules on the surface). Molecules with selenol groups can be cleaved in a different potential window, thus enabling selective cleaving.[35] Selective purification of molecules based on molecular size can also be achieved by well-established techniques to tune the np-Au morphology.[36,37] This novel purification platform combined with the microfabrication compatibility of np-Au should enable the development of multiplexed complete sample-to-answer systems for point-of-care diagnostics.

■ EXPERIMENTAL METHODS

Chemicals and Reagents. Film deposition was performed on 0.15 mm thick glass coverslips (22 mm × 22 mm), which were purchased from Electron Microscopy Sciences. Gold, silver, and chrome targets (99.95% pure) were obtained from Kurt J. Lesker. Nitric acid (70%, used as received) was obtained from Sigma-Aldrich. Sulfuric acid (96%) and hydrogen peroxide (30%) were purchased from and J. T. Baker. Piranha solution, consisting of a 4:1 ratio (by volume) of sulfuric acid and hydrogen peroxide, was used for cleaning glass coverslips. ***CAUTION:*** *Piranha solution and nitric acid are highly corrosive and reactive with organic materials and must be handled with extreme care.* Tris (2-chloroethyl) phosphate (TCEP), magnesium chloride, sodium phosphate monobasic, and sodium phosphate dibasic were obtained from Fisher Scientific. MB was purchased from Sigma-Aldrich. Phosphate-buffered saline (1× PBS), composed of 137 mM NaCl, 2.7 mM KCl, 10 mM Na_2HPO_4, and 1.8 KH_2PO_4 with a pH of 7.4, was obtained from Corning. Heat-inactivated fetal bovine serum (FBS) was obtained from Life Technologies. The oligonucleotides, obtained from Integrated DNA Technologies (IDT), were 26 bases long, and the 5′ end of probe ssDNA was modified with a C6 linker and thiol group. The sequences used in this study were as follows:

Probe ssDNA: 5' ThioMC6-D/CGT GTT ATA AAA TGT AAT TTG GAA TT 3'

Target DNA: 5' AAT TCC AAA TTA CAT TTT ATA ACA CG 3'

Fabrication of Nanoporous Gold Electrodes. Nanoporous gold (np-Au) films were prepared by sputter deposition and subsequent dealloying. Briefly, glass coverslips were cleaned in piranha solution, rinsed in deionized (DI) water, and dried under nitrogen flow prior to metal deposition. Metal deposition was carried out using a magneto-sputtering system (Kurt J. Lesker). First, a 160 nm thick chrome layer was sputtered at 300 W to promote adhesion between glass and the subsequent metallic layers. Next, a 80 nm thick seed layer of gold was sputtered at 400 W, and finally, silver and gold were cosputtered at 200 and 100 W, respectively, to obtain a 600 nm thick alloy layer. All depositions were performed successively under argon ambient at 10 mTorr. The composition of the alloy was 64% Ag and 36% Au (at. %) as determined by X-ray energy dispersive spectroscopy (EDS), (Oxford Instruments). The samples were dealloyed in 70% nitric acid at 55 °C for 15 min to produce the np-Au films and then rinsed with DI water. The substrates were then dealloyed in heated nitric acid, wherein as silver atoms are removed, gold atoms undergo surface diffusion to self-assemble into the characteristic bicontinuous open-pore gold structure.[38] Planar gold (pl-Au) electrodes were also fabricated by sputter-depositing a 50 nm thick chrome adhesion layer followed by 250 nm thick gold film onto piranha-cleaned glass coverslips. Top view and cross-sectional images of np-Au electrode were captured via scanning electron microscope (FEI Nova Nano-SEM430) at 100 k× magnification.

Sensor Preparation. The np-Au and planar gold electrodes were cleaned in dilute piranha solution for 20 s prior to functionalization. The electrodes were then incubated in 25 mM phosphate buffer (PB), containing 2 μM thiolated probe DNA and 50 mM $MgCl_2$, for 15 h at room temperature. Mercaptohexanol (MCH, 1 mM) prepared in PB was used as backfill agent to passivate the surface that was not covered by probe DNA. The electrodes were thoroughly rinsed with PB to remove nonspecifically bound DNA. DNA-functionalized electrodes were incubated in 150 μL of 20 μM MB prepared in 1× phosphate-buffered saline (PBS) for control measurements and in 1× PBS containing 10% fetal bovine serum (FBS) for complex media experiments for 10 min. Unbound MB molecules were removed by washing with PB. The electrode was placed inside a custom-built Teflon electrochemical cell and 1× PBS or 1× PBS containing 10% FBS was used as the electrolyte for measurements. Probe-modified electrode was interrogated with different concentrations of target DNA. The electrode was incubated with desired target DNA prepared in PB containing 50 mM $MgCl_2$ or with the additional 10% FBS (complex media experiments) for 35 min at 37 °C. Nonspecifically bound target molecules were removed by PB rinse. The electrodes were then incubated with MB, and measurements were carried out in a similar fashion as the probe DNA.

Electrochemical Methods. The homemade Teflon cell was utilized to carry out electrochemical measurements with a Gamry Reference 600 potentiostat. np-Au and pl-Au electrodes with footprints of 0.15 cm^2 were employed as working electrodes, whereas platinum wire and Ag/AgCl electrodes were used as counter and reference electrodes, respectively. Probe grafting and target hybridization were electrochemically quantified using the MB−DNA reduction peak obtained via square wave voltammetry (SWV). All SWV measurements were performed in 1× PBS containing 10% FBS

DOI: 10.1021/jacs.6b03563
J. Am. Chem. Soc. 2016, 138, 7711−7717

over the potential range of 0 to −0.5 V with an amplitude of 40 mV, step size of 4 mV, and frequency of 18 Hz for np-Au and 60 Hz for pl-Au. The electrodes were rinsed with PB prior to cleaving. Electrochemical cleaving was done using CV with 25 mM PB as the electrolyte. The potential scan range for CV was between 0 and −1.5 V.

Optical Quantification of Hybrids: PicoGreen Assay. The density of the eluted hybrids was estimated using a fluorescent double-stranded DNA (dsDNA)-binding dye, PicoGreen. Quant-IT PicoGreen dsDNA assay kit was purchased from Thermo Fisher Scientific. PicoGreen dye stock was diluted 200 fold in 1× TE buffer and used as working solution. Standard curves with λ_{DNA} provided were obtained in FBS as shown in Figure S2; 150 μL of eluted hybrids was collected in a microcentrifuge tube. The tube was vortexed lightly and spun down to ensure uniform mixing. A 20 μL aliquot of PicoGreen dye was added to each 20 μL aliquot of the eluted hybrids. At least two different aliquots were analyzed from a single cleaving run. The dye and sample were mixed thoroughly and allowed to equilibrate at room temperature in dark for 5 min. A NanoDrop fluorospectrometer was used for the measurements. PicoGreen exhibits an emission maximum at 530 nm upon binding to dsDNA. A 2 μL sample volume was used for fluorescence quantification. The RFU values were converted to concentration values using the calibration curve in Figure S2.

Capillary Electrophoresis. To evaluate the efficacy of eluted hybrids in the presence of other interfering DNA strands and proteins, capillary electrophoresis was performed before and after purification using Agilent Bioanalyzer 2100. The resulting data is translated into gel-like images (bands) which have been used in this study to evaluate the presence/absence of DNA. The samples before purification contain the target 26 mer DNA along with the other genomic DNA. The eluted samples (after) and the input samples (before) were preconcentrated by centrifugation and evaporation. The obtained concentrations were measured using Thermo Fisher Scientific Qubit, and the concentrations were adjusted such that before and after samples have same similar amounts of DNA. The samples (2 μL) were then loaded onto the bioanalyzer chip.

■ ASSOCIATED CONTENT

Supporting Information

The Supporting Information is available free of charge on the ACS Publications website at DOI: 10.1021/jacs.6b03563.

Additional electrochemical results, PicoGreen optical assay calibration, and electrophoresis results (PDF)

■ AUTHOR INFORMATION

Corresponding Author

*E-mail: eseker@ucdavis.edu.

Notes

The authors declare no competing financial interest.

■ ACKNOWLEDGMENTS

We gratefully acknowledge the support from UC Lab Fees Research Program Award (12-LR-237197), UC Davis Research Investments in the Sciences & Engineering (RISE) Award, and National Science Foundation Awards (CBET-1512745 and CBET&DMR-1454426). We thank Tatiana Dorofeeva for assistance in SEM imaging. We also thank Prof. Josh Hihath, Dr. Paul Feldstein, and Yuanhui Li for discussions on gold−thiol cleaving mechanisms.

■ REFERENCES

(1) Cederquist, K. B.; Kelley, S. O. *Curr. Opin. Chem. Biol.* **2012**, *16*, 415.
(2) Lei, J.; Ju, H. *Chem. Soc. Rev.* **2012**, *41*, 2122.
(3) Zhu, C.; Yang, G.; Li, H.; Du, D.; Lin, Y. *Anal. Chem.* **2015**, *87*, 230.
(4) Xue, Y.; Markmann, J.; Duan, H.; Weissmüller, J.; Huber, P. *Nat. Commun.* **2014**, *5*, 4237.
(5) Tang, S.; Zhang, H.; Lee, H. K. *Anal. Chem.* **2016**, *88*, 228.
(6) Labib, M.; Martić, S.; Shipman, P. O.; Kraatz, H.-B. *Talanta* **2011**, *85*, 770.
(7) Sim, J. H. C.; Anikst, V.; Lohith, A.; Pourmand, N.; Banaei, N. *J. Clin. Microbiol.* **2015**, *53*, 2329.
(8) Price, C. W.; Leslie, D. C.; Landers, J. P. *Lab Chip* **2009**, *9*, 2484.
(9) Sambrook, J.; Russell, D. W. *Molecular Cloning: A Laboratory Manual*; Cold Spring Harbor Laboratory Press: Cold Spring Harbor, NY, 2001; Vol. *1*.
(10) Tian, H.; Hühmer, A. F. R.; Landers, J. P. *Anal. Biochem.* **2000**, *283*, 175.
(11) Breadmore, M. C.; Wolfe, K. A.; Arcibal, I. G.; Leung, W. K.; Dickson, D.; Giordano, B. C.; Power, M. E.; Ferrance, J. P.; Feldman, S. H.; Norris, P. M.; Landers, J. P. *Anal. Chem.* **2003**, *75*, 1880.
(12) Tanaka, N.; Kobayashi, H.; Ishizuka, N.; Minakuchi, H.; Nakanishi, K.; Hosoya, K.; Ikegami, T. *J. Chromatogr. A* **2002**, *965*, 35.
(13) Ishizuka, N.; Minakuchi, H.; Nakanishi, K.; Hirao, K.; Tanaka, N. *Colloids Surf., A* **2001**, *187-188*, 273.
(14) Easley, C. J.; Karlinsey, J. M.; Bienvenue, J. M.; Legendre, L. A.; Roper, M. G.; Feldman, S. H.; Hughes, M. A.; Hewlett, E. L.; Merkel, T. J.; Ferrance, J. P.; Landers, J. P. *Proc. Natl. Acad. Sci. U. S. A.* **2006**, *103*, 19272.
(15) Cady, N. C.; Stelick, S.; Batt, C. A. *Biosens. Bioelectron.* **2003**, *19*, 59.
(16) Reedy, C. R.; Price, C. W.; Sniegowski, J.; Ferrance, J. P.; Begley, M.; Landers, J. P. *Lab Chip* **2011**, *11*, 1603.
(17) Witek, M. A.; Llopis, S. D.; Wheatley, A.; McCarley, R. L.; Soper, S. A. *Nucleic Acids Res.* **2006**, *34*, e74.
(18) Liu, D.; Liang, G.; Zhang, Q.; Chen, B. *Anal. Chem.* **2013**, *85*, 4698.
(19) Clark, K. D.; Nacham, O.; Yu, H.; Li, T.; Yamsek, M. M.; Ronning, D. R.; Anderson, J. L. *Anal. Chem.* **2015**, *87*, 1552.
(20) Alla, A. J.; d'Andrea, F. B.; Bhattarai, J. K.; Cooper, J. A.; Tan, Y. H.; Demchenko, A. V.; Stine, K. J. *J. Chromatogr. A* **2015**, *1423*, 19.
(21) Santos, G. M.; Zhao, F.; Zeng, J.; Li, M.; Shih, W. C. *Journal of biophotonics* **2015**, *8*, 855.
(22) Yin, H.; Zhou, C.; Xu, C.; Liu, P.; Xu, X.; Ding, Y. *J. Phys. Chem. C* **2008**, *112*, 9673.
(23) Daggumati, P.; Matharu, Z.; Wang, L.; Seker, E. *Anal. Chem.* **2015**, *87*, 8618.
(24) Daggumati, P.; Matharu, Z.; Seker, E. *Anal. Chem.* **2015**, *87*, 8149.
(25) Seker, E.; Reed, M. L.; Begley, M. R. *Materials* **2009**, *2*, 2188.
(26) Patel, J.; Radhakrishnan, L.; Zhao, B.; Uppalapati, B.; Daniels, R. C.; Ward, K. R.; Collinson, M. M. *Anal. Chem.* **2013**, *85*, 11610.
(27) Arinaga, K.; Rant, U.; Knežević, J.; Pringsheim, E.; Tornow, M.; Fujita, S.; Abstreiter, G.; Yokoyama, N. *Biosens. Bioelectron.* **2007**, *23*, 326.
(28) Singer, V. L.; Jones, L. J.; Yue, S. T.; Haugland, R. P. *Anal. Biochem.* **1997**, *249*, 228.
(29) Kerman, K.; Ozkan, D.; Kara, P.; Meric, B.; Gooding, J. J.; Ozsoz, M. *Anal. Chim. Acta* **2002**, *462*, 39.
(30) Wang, J.; Rivas, G.; Jiang, M.; Zhang, X. *Langmuir* **1999**, *15*, 6541.
(31) Moore, E. J.; Curtin, M.; Ionita, J.; Maguire, A. R.; Ceccone, G.; Galvin, P. *Anal. Chem.* **2007**, *79*, 2050.
(32) Kurtulus, O.; Daggumati, P.; Seker, E. *Nanoscale* **2014**, *6*, 7062.
(33) Gittard, S. D.; Pierson, B. E.; Ha, C. M.; Wu, C. A. M.; Narayan, R. J.; Robinson, D. B. *Biotechnol. J.* **2010**, *5*, 192.
(34) Yeates, C.; Gillings, M.; Davison, A.; Altavilla, N.; Veal, D. *Biol. Proced. Online* **1998**, *1*, 40.
(35) Sato, Y.; Mizutani, F. *Phys. Chem. Chem. Phys.* **2004**, *6*, 1328.
(36) Tan, Y. H.; Davis, J. A.; Fujikawa, K.; Ganesh, N. V.; Demchenko, A. V.; Stine, K. J. *J. Mater. Chem.* **2012**, *22*, 6733.
(37) Dorofeeva, T.; Matharu, Z.; Daggumati, P.; Seker, E. *J. Phys. Chem. C* **2016**, *120*, 4080.

DOI: 10.1021/jacs.6b03563
J. Am. Chem. Soc. 2016, 138, 7711−7717

(38) Erlebacher, J.; Aziz, M. J.; Karma, A.; Dimitrov, N.; Sieradzki, K. *Nature* **2001**, *410*, 450.

DOI: 10.1021/jacs.6b03563
J. Am. Chem. Soc. 2016, 138, 7711−7717